



# The 3D-Printing Technology of Geological Models Using Rock-Like Materials

Xia-Ting Feng<sup>1</sup> · Yan-Hua Gong<sup>1</sup> · Yang-Yi Zhou<sup>1</sup> · Zheng-Wei Li<sup>1</sup> · Xu-Feng Liu<sup>1</sup>

Received: 19 June 2018 / Accepted: 11 December 2018 / Published online: 9 January 2019  
© Springer-Verlag GmbH Austria, part of Springer Nature 2019

## Abstract

The common practice in understanding some puzzling geotechnical and geomechanical issues by large-scale three-dimensional physical model tests is recently much improved by the introduction of 3D-printing technology which can realize the reconstruction of complex geological structures. However, during 3D printing process, the regular rock-like material suffers from some general problems such as short initial setting time, water segregation, decreasing fluidity induced by chemical reaction, and some other unclear influencing factors. To promote further development of physical model via 3D printing method and to fabricate large-scale high-precision 3D geological models, in this paper, the flow characteristics of rock-like materials were first investigated using a new fluidity testing apparatus. Based on the test results, a novel 3D-printing technology of geological material was formulated. Then, the technologies of fabricating the desired structural specimens, acquiring samples with mechanical properties and cracking behaviors similar to natural rock, printing large-scale complex geological models were formulated. The results show that the 3D-printing technology of geological materials had a principle: no losing fluidity during printing time. The parameters of print head diameter, line width, line span, and line slump were the four key factors affecting desired structural samples. From the enlightenment of printing small-scale sample, the printing methods of complex large-scale geological models including decreasing printing time, acquiring heterogeneous geological model with inner structures, desired density, and surrounding smooth surface were proposed.

**Keywords** Rock-like materials · 3D-printing technology · Desired structural specimens · Mechanical properties · Cracking behaviors

## 1 Introduction

Geological model with complex structure test is an important way to visualize certain engineering problems (Feng et al. 2017). So far, there are mainly three methods used to construct geological models: pouring, tamping, and small block masonry (Liu et al. 2013; Zhang et al. 2015). However, several disadvantages arise when using these artificial methods, including being unable to simulate detailed tectonic discontinuities (Zhang et al. 2015; Chen et al. 2015; Fumagalli 1966), difficulty in guaranteeing uniformity of the density of different layers (Zhu et al. 2010, 2011; Li et al.

2015), and bringing in additional contact surfaces (Liu et al. 2013; Ma et al. 2017).

3D-printing technology, also known as additive manufacturing, provides a novel way to solve afore mentioned shortcomings by slicing and printing complex models layer-by-layer. Ju et al. (2017a, b) use aggregated materials to print transparent structural samples for acquiring stress field data. They have also printed heterogeneous rock samples with complex structures based on X-ray microfocus computed tomography (Ju et al. 2014, 2017; Liu et al. 2016). Jiang et al. (2016) and Xiong et al. (2015) utilize a 3D scanner to get surface data from natural rock joints. The rock joint model based on scanning data was then printed using a polylactic acid (PLA) printer. At last, the same rock joint samples are manufactured by pouring method. Wang et al. (2017) print a fractured network using a PLA printer and put it with similar materials into a mould to make a fractured rock sample. Jiang and Zhao (2015) demonstrate that the compressive properties of PLA samples are plastic. Powder-based 3D

✉ Xia-Ting Feng  
xtfeng@whrsm.ac.cn

<sup>1</sup> Key Laboratory of Ministry of Education on Safe Mining of Deep Metal Mines, Northeastern University, Shenyang 110819, Liaoning, China

printers are the most widely used apparatus in rock modelling. Using this type of printer, Fereshtenejad and Song (2016) find that the strength of printed samples is influenced by printing direction, layer thickness, heating, and binder saturation level. Jiang et al. (2016a, b, c) investigate the tensile mechanical properties of printing samples with pre-set cracks. They find that the crack failure mode of printed samples is similar to that of Portland cement concrete samples. Tian and Han (2017) test the failure mode of printed samples with different angles of pre-existing flaws under uniaxial compressive conditions. The experiment shows that the mechanical properties of printed specimens are similar to rock-type materials. Shakor et al. (2017) develop a water-based binder-printing method to instead the glue-based binder-printing method. The results indicate that the mechanical properties of 3D-printed samples are enhanced using this method. Vogler et al. (2017) compare the tensile strength of artificial sandstone specimens with 3D-printed specimens and find that the indirect strength, surface roughness, and crack propagation behavior of printed samples are similar to those of a weak natural sandstone. Bauyrzhan et al. (2017) investigate the temperature dependence and find that the unconfined compressive strength of 3D-printed samples decreases from 19 to 1.1 MPa when the temperature increases from 25 °C to 80 °C. In addition, Zhou and Zhu (2017, 2018) investigate the suitability of ceramics, gypsum, PMMA, SR20, and resin to simulate brittle, hard rock. The results indicate that the resin is the most suitable material, but its brittleness remains to be improved.

In spite of having the ability to produce complex structures, there are still some disadvantages for 3D-printing geological models using universal rock-like materials. The printing method used in constructing rock-like samples mainly have four categories: fused deposition modelling (FDM), three-dimensional printing and gluing (3DP), stereolithography apparatus (SLA), and selective laser sintering (SLS). FDM is a 3D-printing technology based on hot extrusion. The printing materials require a lower melting point and cold welding in subsequent layers (Huang et al. 2013; Kruth et al. 1998; Pham and Gault 1998). 3DP is a kind of technology that utilizes a nozzle for selective gluing of powdered material (Chia and Wu 2015; Otten et al. 2012; Yan and Gu 1996). SLA adopts a UV laser to irradiate a photosensitive resin. The liquid resin will solidify when the laser irradiate the resin surface (Melchels et al. 2010; Mondschein et al. 2017; Skawinski et al. 1995; Weng et al. 2016). SLS has some similarities to 3DP except the printer. The build material is fused under high power laser (Launhardt et al. 2016; Fina et al. 2017). Unlike these novel 3D printing methods, geological materials are solidifying through its chemical reaction. Geological materials can be divided into two categories: cementing materials and aggregates (Cao et al. 2018). The challenge of 3D-printing geological materials is

that cementing materials and aggregates are always mixed together with water and solidify over time.

In this paper, the 3D-printing disadvantages with geological materials were first investigated with a new fluidity testing apparatus. After that, some measures were developed to solve these problems. Then, the technologies of producing desired structural specimens, acquiring samples with mechanical properties and cracking behaviors similar to natural rock, and printing large-scale complex geological models were analyzed.

## 2 Materials and Experiments' Methods

### 2.1 Materials

The 3D-printing technology used for cementitious materials needs to meet the following requirements: setting time, extrudability, flowability, and desired strength (Ma et al. 2017). To ensure the geological materials with good workability and printable performance, the test materials including silica sand, two types of cement, and two types of gypsum, which are frequently used in geological models, were prepared. Two types of cement and two types of gypsum were selected to ensure that the test results were suitable for other cementitious materials. Two types of set retarder and a kind of water-retaining agent were used to increase initial setting time and avoid segregation, respectively. Their detailed information is shown in Table 1.

### 2.2 Experiment Methods

#### 2.2.1 Initial Setting Time Measurement

Initial setting time was an important factor influencing the fluidity of cementitious materials (Tan et al. 2018). It was assessed with the Vicat apparatus (Fig. 1). The initial setting time was measured under normal consistency conditions. The steel needle diameter used to test initial setting time was 1.13 mm. The initial setting time was measured every 10 s for high-strength gypsum with its initial setting time less than 3 min. The initial setting time of the other cementing materials was tested every 30 min, at first. When approaching the initial setting time, it was tested every 1 min. When the distance from the needle head to the lowest point was less than 5 mm, the testing time was determined as the initial setting time. All the tests were conducted at 20 °C.

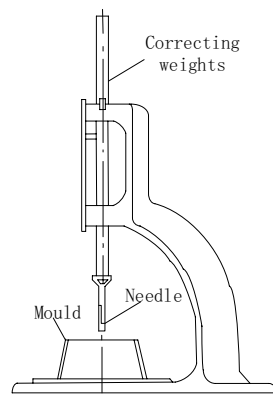
#### 2.2.2 Fluidity Measurement

Flowmeters can be divided into three categories based on its measuring principles: volumetric flowmeters, velocity-type flowmeters, and mass flowmeters (Jin et al. 2017). The flow

**Table 1** Source information of testing materials

Materials	Company	Location
Caulking gypsum	Shenyang 303 Decorative Ltd	Shenyang, China
High-strength gypsum	Shenyang Li-shi-jia Ltd	Shenyang, China
325 Slag Portland cement	Shenyang Shan-shui Cement Ltd	Shenyang, China
525 Portland cement	Tangshan Ji-dong Cement Ltd	Tangshan, China
Silica sand	Shenyang Xin-jiu-wang Trading Ltd	Shenyang, China
Sodium polyphosphate	Shandong Le-gao Environmental and Technology Ltd	Qingdao, China
Sodium gluconate	Tianjin Bei-chen-fang-zheng Chemical reagent factory	Tianjin, China
Hydroxypropyl methyl cellulose	Hebei Qing-jun cellulose factory	Shijiazhuang, China

**Fig. 1** Initial setting time test



characteristics of geological materials were difficult to assess by universal flowmeter, because there were some unique characteristics on testing the fluidity of cementitious materials such as varied initial setting time and water segregation (Bryan et al. 2015a, b; Khelifi et al. 2013). Based on flowmeter test principles and the flow characteristics of geological materials, a novel fluidity testing apparatus that consisted

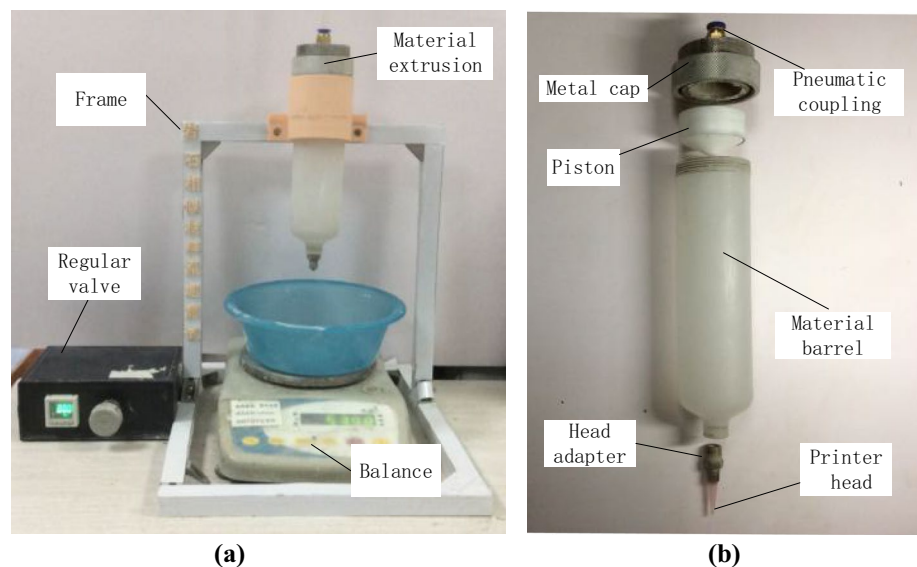
of frame, material extrusion, regular valve, electronic balance, and air pump was developed (Fig. 2a). The material extrusion that consisted of pneumatic coupling, metal cap, piston, material barrel, head adapter and printer head was used to contain and squeeze out the test materials (Fig. 2b).

The general procedures for testing the fluidity of cementitious materials were as follows. First, the needle adapter was mounted on the material barrel. To eliminate air, the mixture was vibrated on a shaking table. Subsequently, the piston, metal cap, and needle were mounted by turn. Second, material extrusion was positioned on frame. The material extrusion and regular valve were connected with high-pressure plastic pipe. In the end, the testing began with the target air pressure adjusted via the regular valve. The balance data were recorded and stored per minute.

### 2.2.3 Influencing Parameter Measurement

The parameters of line width, line span, and line slump are the main factors that affect printing precision (Lanaro et al. 2017; Lille et al. 2018; Yang et al. 2018). To investigate the

**Fig. 2** Fluidity test; **a** fluidity test apparatus; **b** material extrusion



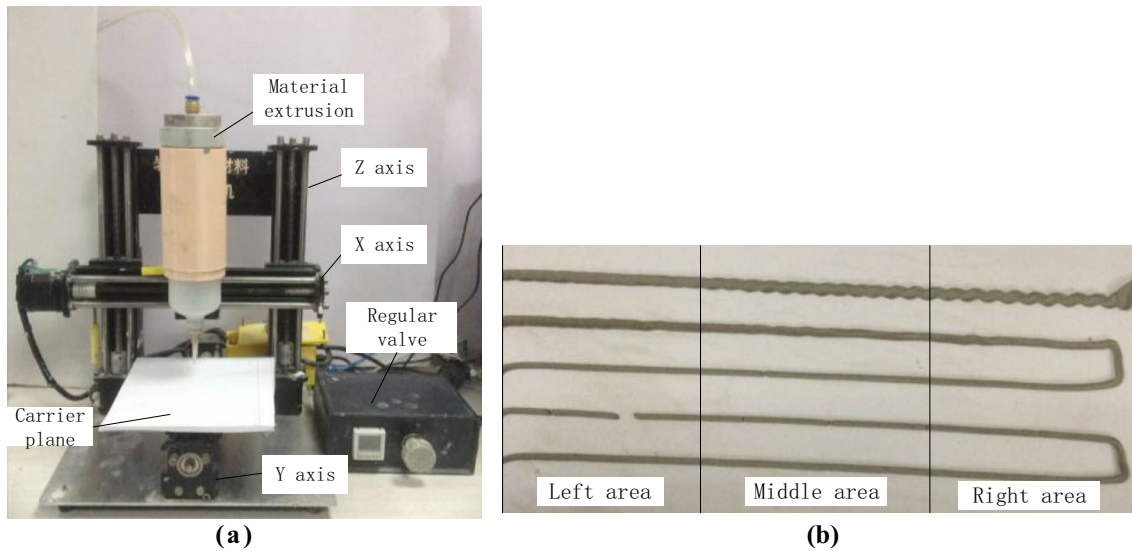


**Fig. 3** Line width test; **a** line width testing apparatus; **b** printed line

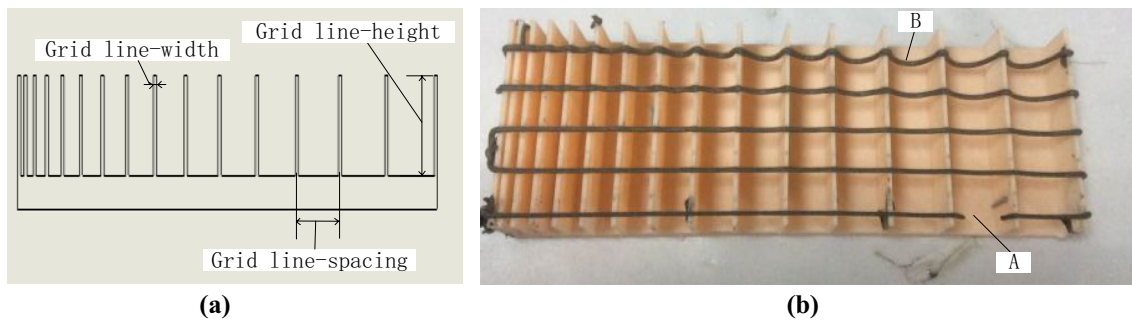


**Fig. 4** Line span test method; **a** line span testing apparatus; **b** sketch map of printed line; A—line collapse, B—line fracture

influencing line width factors, a new kind of test apparatus was developed. The device consisted of extruder, carrier plane, regular valve, air pump, and moving axis. The material extrusion moved along with the X- and Z-axes and the carrier plane moved along with the Y-axis (Fig. 3). To investigate the influencing line span factors, different interval grids were printed using a PLA 3D printer. Their distance changed from 1 to 15 mm (Fig. 4a). The test principle was that a printed line on the grid surface would collapse or fracture due to gravity. The line span had the following evaluation standards: (1) the line collapse by more than 1 mm and (2) the line fractured. To investigate factors influencing line slump, a printing routine of rectangle frame, 50 mm × 50 mm, was designed to obtain the slump height (Fig. 5a). The test principle was that the frame would break down with increasing height (Fig. 5b).

The general procedures for investigating the factors influencing line width included the following basic steps: (1) charging materials. The test materials were poured into the

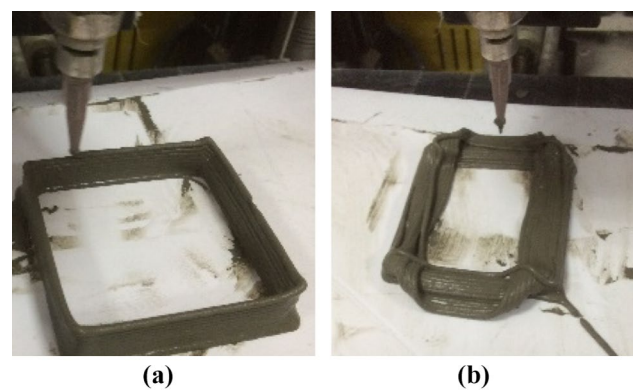


**Fig. 5** Printing material slump test method; **a** rectangle line printing process; **b** printing rectangle slumped shape

material extrusion with vibrating on the shaking table. (2) Designing movement routine. The test began when the air pressure reached the target pressure. The printer head would



move under computer controlling. (3) Measuring the line width. The printed lines were divided into three parts: left, middle, and right. The line width value was taken as the average width after measuring each area once.

The general procedures for investigating the factors influencing line span included the following basic steps: (1) charging materials; (2) putting the line slump onto the carrier plane. The long side of the line span testing apparatus was paralleling to  $X$ -axis; (3) design movement routine; and (4) measuring the line span. When the collapse height was more than 1 mm or fractured, the line slump value was taken as the previous grid width.

The general procedures for investigating the factors influencing line slump included the following basic steps: (1) charging materials; (2) designing movement routine; and (3) testing the line slump. The line slump value was taken as the rectangle height before it broken down.

#### 2.2.4 Geological Material 3D Printer

Based on extrusion technology, a new small-scale geological material 3D printer was developed (Khoshnevis and Bekey 2002; Gosselin et al. 2016; Kazemian et al. 2017). This device consisted of printing controller, printing frame, extrusion controller, material container, regular valve, and air pump (Fig. 6). The printing software named Repetier was used to control the printing process. The print head moved freely along the  $X$ - and  $Y$ -axes and the printing platform moved along with  $Y$ -axis. The air pressure controlled by the regular valve impelled geological materials into the extrusion controller.

The printing procedures of this printer were as follows. (1) preparing printing model. A digital model constructed by 3D model designing software and sliced by Slic3r (a kind of open source software was used to slice the digital models

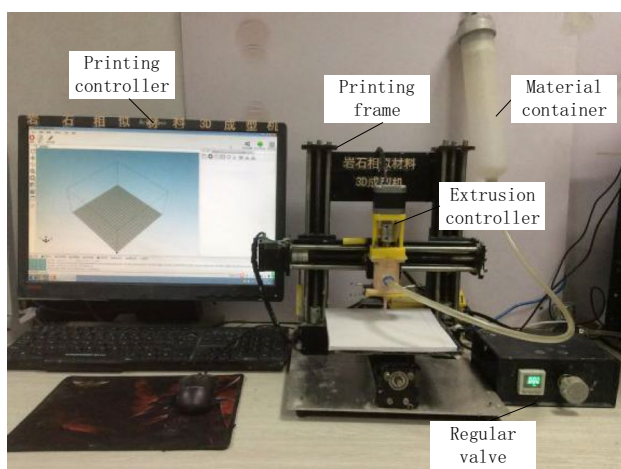


Fig. 6 Geological material 3D printer

into routine data). (2) Cleaning extrusion controller. The extrusion controller needs to be cleaned to decrease the initial flow resistance and avoid blocking print head. (3) Model printing. Some basic printing parameters including fill density, print speed, layer height, and nozzle diameter should be set before slicing the virtual model. In our experiment, the fill density, print speed, layer height, and nozzle diameter were 100%, 60 mm/s, 1 mm, and 1.4 mm, respectively. (4) Post-treatment. The 3D-printed samples with Portland cement were maintained 30 days under the temperature of 20 °C and relative humidity of 90%, and the gypsum samples were maintained 7 days at the temperature of 20 °C in dry air.

### 3 Results

Geological materials utilized to manufacture different kinds of geological models usually can be divided into three main categories: cementing materials, aggregate, and additive agent. Because the fluidity of aggregate remained stable during printing process, the main challenges affecting normal printing process are the properties of cementing materials. Therefore, the printing disadvantages using cementing materials were investigated and some measures were proposed to solve these problems. Then, the fluidity affected by water, set retarder, water-retaining admixture, and air pressure was investigated. Based on these results, the 3D-printing technology of geological materials was established.

#### 3.1 Flow Characteristics

The 3D-printing technology of cementing materials needs to meet the following requirements: proper setting time, extrudability, flowability, and desired strength (Ma et al. 2017). To obtain cementing material flow features, two types of cement and two types of gypsum, which used frequently as cementing materials in geological models, were tested. When combined with water, the high-strength gypsum solidified rapidly in 1 min and released lots of heat. Due to such short initial setting time, the gypsum would solidify during mixed with water and no enough time to be printed (Fig. 7a). When the two types of cement were combined with water, rapid solidifying phenomenon did not occurred in 2 h. However, during testing cement flow features using the fluidity testing apparatus (Fig. 2), the cement flow normally at first. When the cement approached cessation of flow, the extrusion began to bleed water. After no fluidity, when the testing materials were took out from the extrusion container (Fig. 7b), the results indicated that only partial inner materials were running out. With bleeding water and inner materials running out, we got the conclusion that the cement occurred water segregation. When combining with

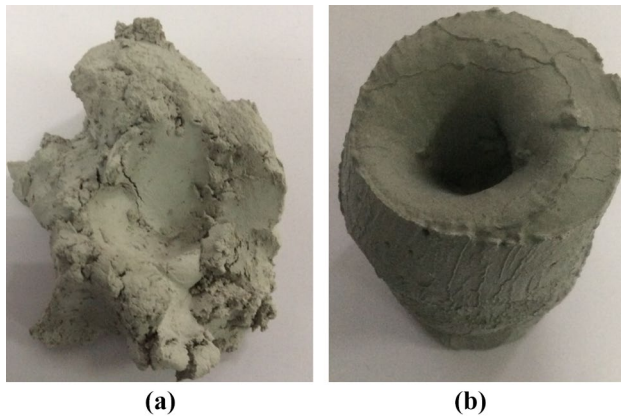


**Fig. 7** Geological disadvantages test; **a** rapid solidification; **b** water segregation

set retarder, the high-strength gypsum also occurred water segregation phenomenon. While testing caulking gypsum, the phenomenon of rapid solidification and water segregation did not occurred.

### 3.2 Solutions for Rapid Solidification and Water Segregation

During testing the flow features of caulking gypsum, the phenomenon of rapid solidification and water segregation did not occur. Referencing to correlative literatures, the caulking gypsum was mixed with set retarder and water-retaining admixture to solve rapid solidification and water segregation. For other cementing materials, the advantageous effect of set retarder and water-retaining admixture was investigated in the following test. Sodium gluconate and sodium polyphosphate were used as the setting retarder for

gypsum and cement, respectively. Hydroxypropyl methyl cellulose was used as a water-retaining admixture.

In this section, the standard water requirements for normal consistency were measured using initial setting apparatus, and the value of high-strength gypsum, 325R slag Portland cement, and 525R ordinary Portland cement was 178 g, 148 g, and 170 g, respectively. Subsequently, the initial setting time was tested, and the values were 1 min, 343 min, and 235 min, respectively. At last, the order of admixture effect was tested. The detailed effects are shown in Table 2. For the setting retarder, the best order of the addition of high-strength, 325R slag Portland cement, and 525R Portland cement was simultaneous mixing, later mixing and later mixing, respectively. For the water-retaining agent, this order was first mixing, later mixing, and later mixing. The admixture used in following tests was mixed with the optimal order of addition.

Figure 8 shows the influence of retarder addition on the initial setting time. For two types of cement, the initial setting time almost increased six times when the setting retarder dose was increased from 0 to 0.75 g. For high-strength gypsum, the initial setting time increased from 1 min to 680 min when the setting retarder dose increased from 0.5 to 3 g. These results indicated that setting retarder could increase the initial setting time of cementitious materials. Compared with high-strength gypsum, the cement was sensitive to setting retarder on increasing initial setting time.

In the end, by adding suitable dose of setting retarder and water-retaining mixture to cementing materials, the high-strength gypsum, 325R slag Portland cement, and 525R ordinary Portland cement did not appeared rapid solidification, bleeding water, and running out inner materials, as shown in Fig. 7. The results indicated that the rapid solidification and water segregation could be solved by adding

**Table 2** Setting retarder adding order effect

Materials	Mixing method	Standard water demand (g)	Setting retarder (g)	Initial setting time (min)	Water-retaining agent (g)	Initial setting time (min)
High-strength gypsum	No mixing	178	0	1	0	38
	First mixing		0.5	4	1	68
	Simultaneous mixing		0.5	16	1	44
	Later mixing		0.5	3	1	49
325R Slag Portland cement	No mixing	148	0	343	0	540
	First mixing		0.15	410	1	433
	Simultaneous mixing		0.15	360	1	523
	Later mixing		0.15	428	1	545
525R Ordinary Portland cement	No mixing	170	0	235	0	286
	First mixing		0.15	309	1	204
	Simultaneous mixing		0.15	10	1	381
	Later mixing		0.15	386	1	388

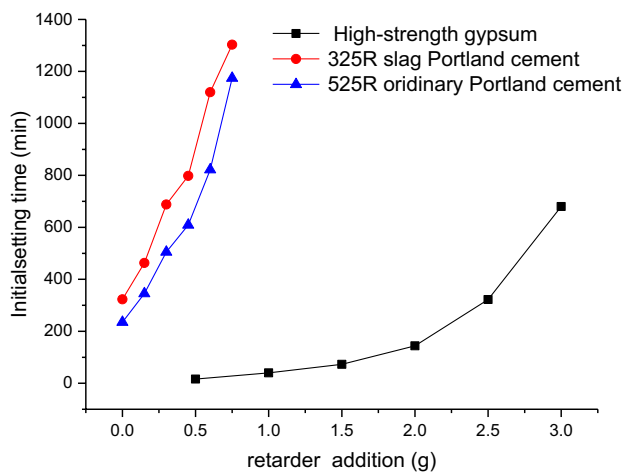


Fig. 8 Retarder addition influencing on initial setting time

suitable dose of set retarder and water-retaining admixture with cementing materials.

### 3.3 Printing Method

Given that, set retarder and water-retaining admixture could solve the rapid solidification and water segregation of cementing materials. The influence of set retarder, water-retaining admixture, and air pressure on the sustaining flow characteristics of cementing materials was studied.

Figure 9 illustrates that the set retarder influence on sustaining stable fluidity of cementing material. The water cement ratio of high-strength gypsum, 325R slag Portland cement, and 525R Portland cement was 0.43, 0.3, and 0.36, respectively. The air pressure kept invariant during

whole test process and the respective initial pressure were 0.08 MPa, 0.05 MPa, and 0.05 MPa separately. As shown in Fig. 9a, the results demonstrated that the cementing material’s fluidity was in positive correlation with set retarder addition. However, the fluidity of 525R ordinary Portland cement was more sensitive to set retarder than the other two types of cementing materials. As shown in Fig. 9b, the continual flow ability of cementing materials was tested with the set retarder addition of 3 g, 0.5 g, and 0.5 g, respectively. The fluidity of high-strength gypsum and 325R slag Portland cement almost kept stable at first and decreased sharply to zero in last 1 min. The fluidity of 525R Portland cement decreased to zero at 8 min. These results indicated that the set retarder had a positive affection on sustaining stable fluidity of cementing materials. However, the cementing materials occurred water segregation phenomenon in this test process due to no adding water-retaining admixture.

Figure 10 shows that the influence of water-retaining admixture on sustaining stable fluidity of cementing material. The addition of water cement ratio and set retarder was the same, as described in Fig. 9. The air pressure kept invariant during whole test process and the initial pressure was 0.1 MPa, 0.06 MPa, and 0.06 MPa, respectively. As shown in Fig. 10a, the fluidity of high-strength gypsum and 525R ordinary Portland cement reached maximum at 2 g and 1.6 g. However, the fluidity of 325R slag Portland cement decreased when water-retaining admixture increased. As shown in Fig. 10b, the continual flow ability of 325R slag Portland cement, high-strength gypsum, and 525R ordinary Portland cement detected with set retarder addition 0.8 g, 2 g, and 1.6 g separately. Their fluidity all decreased, but the water segregation did not occurred and the continual flow time were much longer than only adding

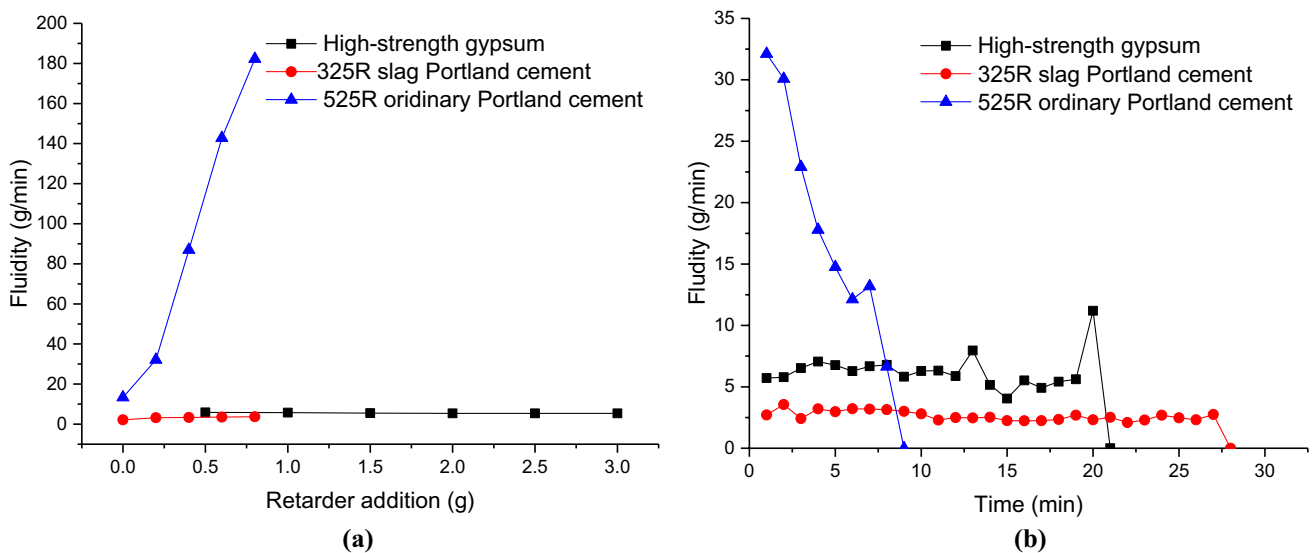
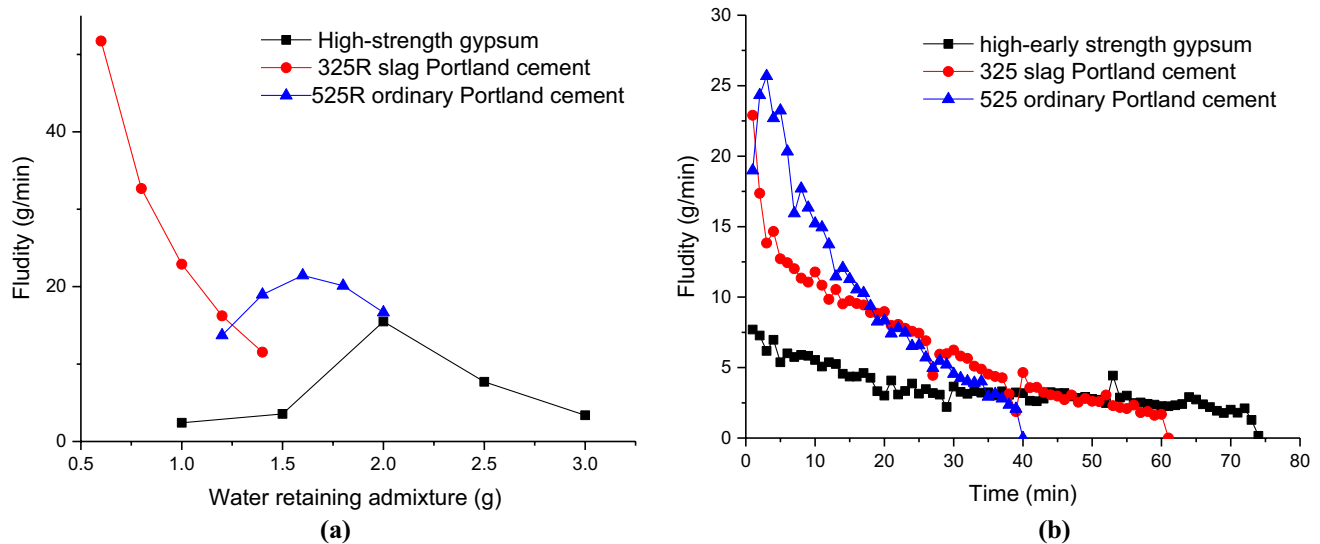


Fig. 9 Flowing characteristics after adding retarder; a retarder addition influencing; b time influencing



**Fig. 10** Flowing characteristics after adding setting retarder and water-retaining agent; **a** water-retaining agent influencing; **b** time influencing

set retarder. These results proved that the water-retaining admixture had a positive affection on sustaining stable fluidity of cementing materials, and the method of adding water-retaining admixture could solve water segregation of cementing materials.

Figure 11 expresses that the influence of increasing air pressure on sustaining stable fluidity of cementing material. The addition of water cement ratio, set retarder, and water-retaining admixture was the same, as described in Fig. 10. The caulking gypsum only mixed with 165 g of water. The flow-state evolution of caulking gypsum, high-strength gypsum, 325R slag Portland cement, and 525R ordinary Portland cement is shown in Fig. 11a–d, respectively. With initial air pressure, the fluidity of all cementing materials decreased with time. When increasing the air pressure, the fluidity rapidly increased. After reaching the peak fluidity, the fluidity began to decrease thereafter. These results indicated that the fluidity decreased over time and would maintain within a certain rang by increasing air pressure. However, increasing the air pressure had no obvious influence on fluidity when the flow time approached the cementing material initial setting time.

Based on the above discussions, the 3D-printing technology of geological materials could be summarized as follows. First, when selecting cement or gypsum as cementing material, the initial setting time needs to be increased by adding proper dose of set retarder. Second, the water-retaining admixture should be added into cementing materials for avoiding water segregation. At last, the driving air pressure must keep continuous increasing for compensating enhance flow resistance caused by chemical reaction of cementing materials over time.

## 4 Discussion

The 3D-printing technology of geological materials is summarized in Sect. 3. However, there were still three key problems need to be solved. One was how to produce the desired structural specimen. Another was how to use 3D-printing technology to prepare rock-like samples that would have mechanical properties and cracking behaviors similar to natural rock. The last was how to print large-scale complex geological models.

### 4.1 Printing Method of Desired Structural Samples

The parameters of print head diameter, line width, line span, and line slump were the four important factors affecting desired structural samples. The print resolution that decided the minimum size of printed structures affected by the printer head diameter. The line interval was determined by line width. The line span decided the impending length of model inner holes. The line slump was the maximal printed height with continuous printing ability. To acquire desired structural samples, the factors influencing the print head diameter were firstly investigated. Then, the factors influencing line width, line span, and line slump were investigated. At last, printing technology of desired structural samples was formulated.



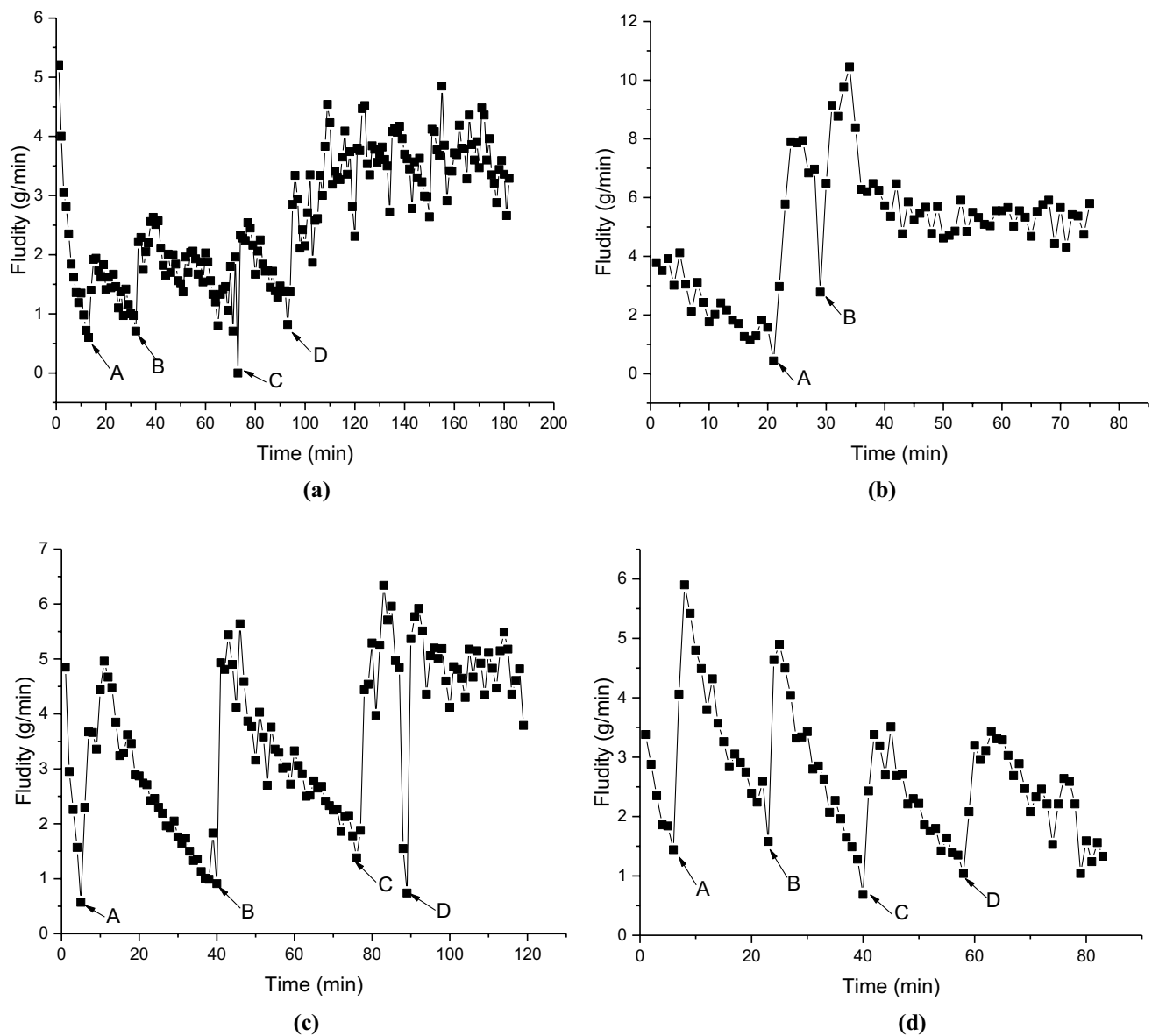


**Fig. 11** Flowing characteristics by increasing air pressure; **a** caulking gypsum; **b** high early strength gypsum; **c** 325R slag Portland cement; **d** 525R ordinary Portland cement; A, B, C, and D point increase air pressure

#### 4.1.1 Print Head Diameter

Print head diameter was an important parameter influencing printing resolution. The aggregates of geological materials, such as silica, did not undergo chemical reaction, but influence the printing head diameter. Therefore, we just chose silica from geological aggregates for test purpose. In this section, 325R slag Portland cement and silica selected as the testing materials. The mass of cement, silica, and water was 500 g, 100 g, and 180 g, respectively. The added dose of setting retarder and water-retaining agent were 0.5 g and 1 g, respectively. The maximum granular size

of silica was less than 0.28 mm. The different print head diameters were 0.9 mm, 1 mm, 1.2 mm, and 1.5 mm.

To find out the influencing factors of print head diameter, the flow characteristics were investigated using different sizes of print head. Table 3 shows the cement fluidity with different print head diameters and air pressures. With a 0.9 mm diameter print head, the cement did not flow no matter how much the air pressure increased. When the print head diameter was 1 mm or 1.2 mm, the cement stopped thrice and once during test, respectively. However, when the print head diameter was 1.5 mm, the cement kept continuous flowing. The results indicated that the print head

**Table 3** Printer head diameter trials

Printer head diameter 0.9 mm		Printer head diameter 1 mm		Printer head diameter 1.2 mm		Printer head diameter 1.5 mm	
Pressure (MPa)	Velocity (g/s)	Pressure (MPa)	Fluidity (g/s)	Pressure (MPa)	Velocity (g/s)	Pressure (MPa)	Velocity (g/s)
Process description		Process description		Process description		Process description	
0.1	—	0.26	9.59	0.205	5.09	0.165	5.87
0.2	—	0.275	10.24	0.215	7.52	0.175	8.2
0.3	—	0.285	12.49	0.225	8.46	0.185	9.66
0.4	—	0.295	13.56	0.235	10.82	0.195	10.08
0.5	—	0.305	13.64	0.245	11.43	0.205	12.34
	Non-fluidity		Suspend				
	Non-fluidity		Suspend				
	Non-fluidity		Suspend		Suspend		
	Non-fluidity		Suspend				
	Non-fluidity						

diameter should be five times bigger than the particle size of aggregates.

**4.1.2 Line Width, Line Span, and Line Slump**

The parameters of line width, line span, and line slump were the other factors influencing the printing consequences of desired structural samples. In this section, the factors of affecting line width, line span, and line slump were investigated. When no investigating the influencing factors, the mass of cement, air pressure, printer head diameter, water addition, printing speed, setting retarder, and water-retaining agent was 500 g, 0.1 MPa, 1.4 mm, 180 g, 60 mm/s, 0.8 g, and 1 g, respectively. In the benchmark experiment, the detailed information of changing factors is shown in Table 4.

Figure 12 shows the factors influencing on line width. The results indicated that air pressure, print head diameter, water addition, and set retarder could increase the line width. However, the line width would decrease when printing speed and water-retaining admixture increased. Because the line interval was decided by line width, the choosing principles of proper parameter for line interval were as follows. Once the print head diameter selected, the maximum printing precision was determined. To acquire best printing precision, we should selected the other parameter values that correspond to the print head diameter. Figure 13 shows the factors influencing on line span. The air pressure promoted line span in a certain range and the head diameter and water-retaining admixture had a positive affection online span. However, the line span would decrease with the increasing of water addition, printing speed, and set retarder. Because impending length for manufacturing inner holes was decided by line span, the longer line span was, the larger impending hole was obtained. Therefore, the choosing principles of proper parameters for line span were that how to increased line span length. Figure 14 shows the factors influencing slump. The influencing factors excepted printing speed had a positive affection on line slump. Because continuous printing ability decided by line slump, the choosing principles of proper parameters were increasing data value of positive influencing parameters and decreasing data value of negative parameter.

**4.1.3 Methods**

The parameters of print head diameter, line width, line span, and line slump were the four key factors affecting desired structural samples. The printing method of desired structural sample was summarized as follows. First, printing resolution was determined by the size of aggregates. In terms of this theory, the printing resolution could increase limitlessly as long as the print head diameter was five times bigger than aggregate size. Second, to further

**Table 4** Changed scope of influencing factors for print parameter

Print parameter	Air pressure (MPa)	Print head diameter (mm)	Water addition (g)	Printing speed (mm/s)	Setting retarder (g)	Water-retaining admixture (g)
Line width	0.09–0.13	1–1.8	165–187	20–60	0–0.8	0.8–1.6
Line span	0.12–0.16	1–1.8	165–187	20–33	0–0.8	0.6–1.4
Line slump	0.175–0.215	1–1.8	165–187	20–60	0–0.8	0.6–1.4

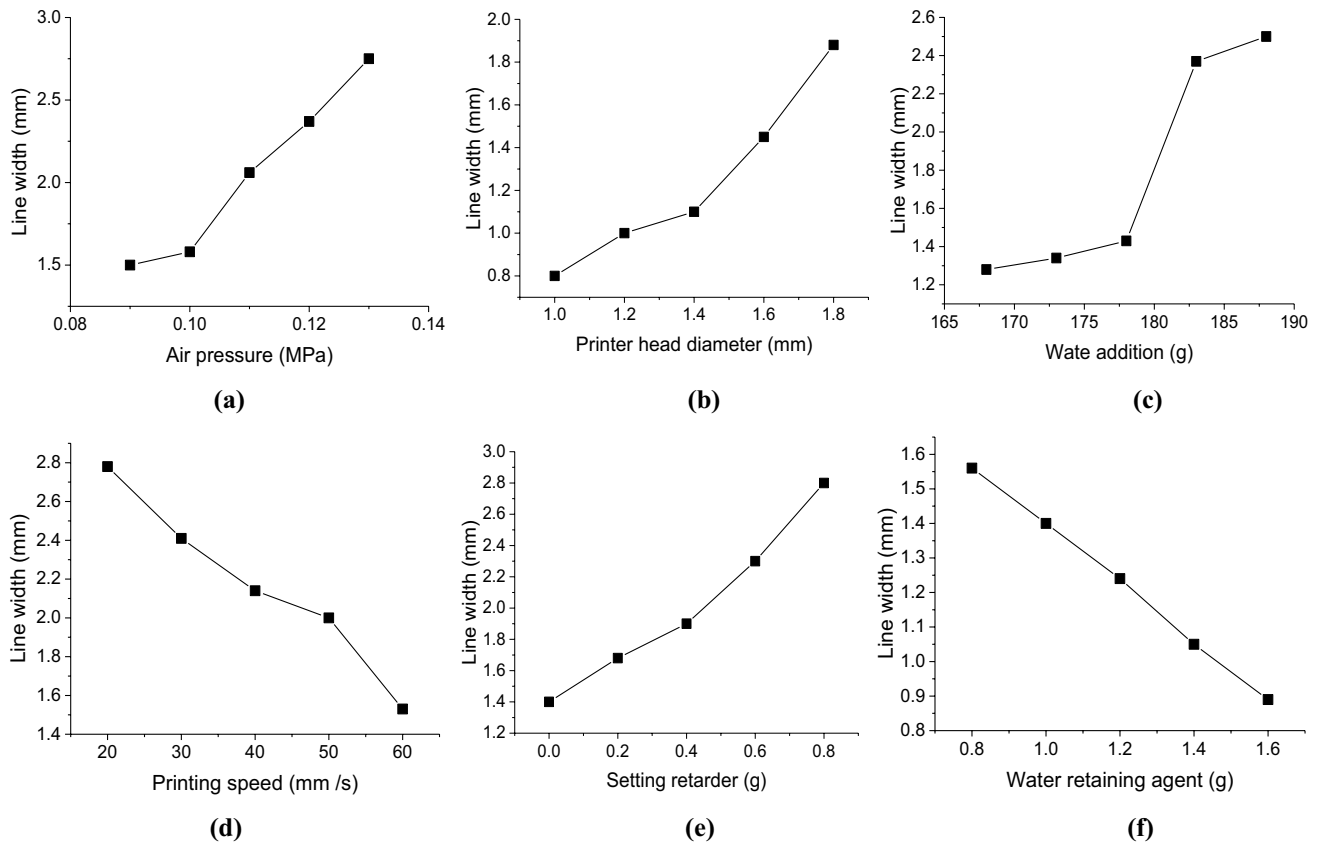


**Fig. 12** Line span influence factor; **a** air pressure; **b** printer head diameter; **c** water addition; **d** printing speed; **e** setting retarder; **f** water-retaining agent

improve the print precision, the line width needs to be near the print head diameter. The influencing parameters were selected, as the values corresponded the print head diameter. Third, the line span determined the impending length of samples inner hole. If there no hole in printing sample, the parameter did not need to be consideration. The last was that the printing height must be lower than line slump height. When approaching maximum line slump value, the printing process should suspend until the printed parts had solidified.

### 4.2 Potential Application

In this section, the potential application of printed samples with rock-like materials was investigated. First, the printed surface characteristics of caulking gypsum, high-strength gypsum, 325R slag Portland cement, and 525R ordinary Portland cement were analyzed. Then, the mechanical properties and cracking behaviors of printed samples were contrasted with natural rock.

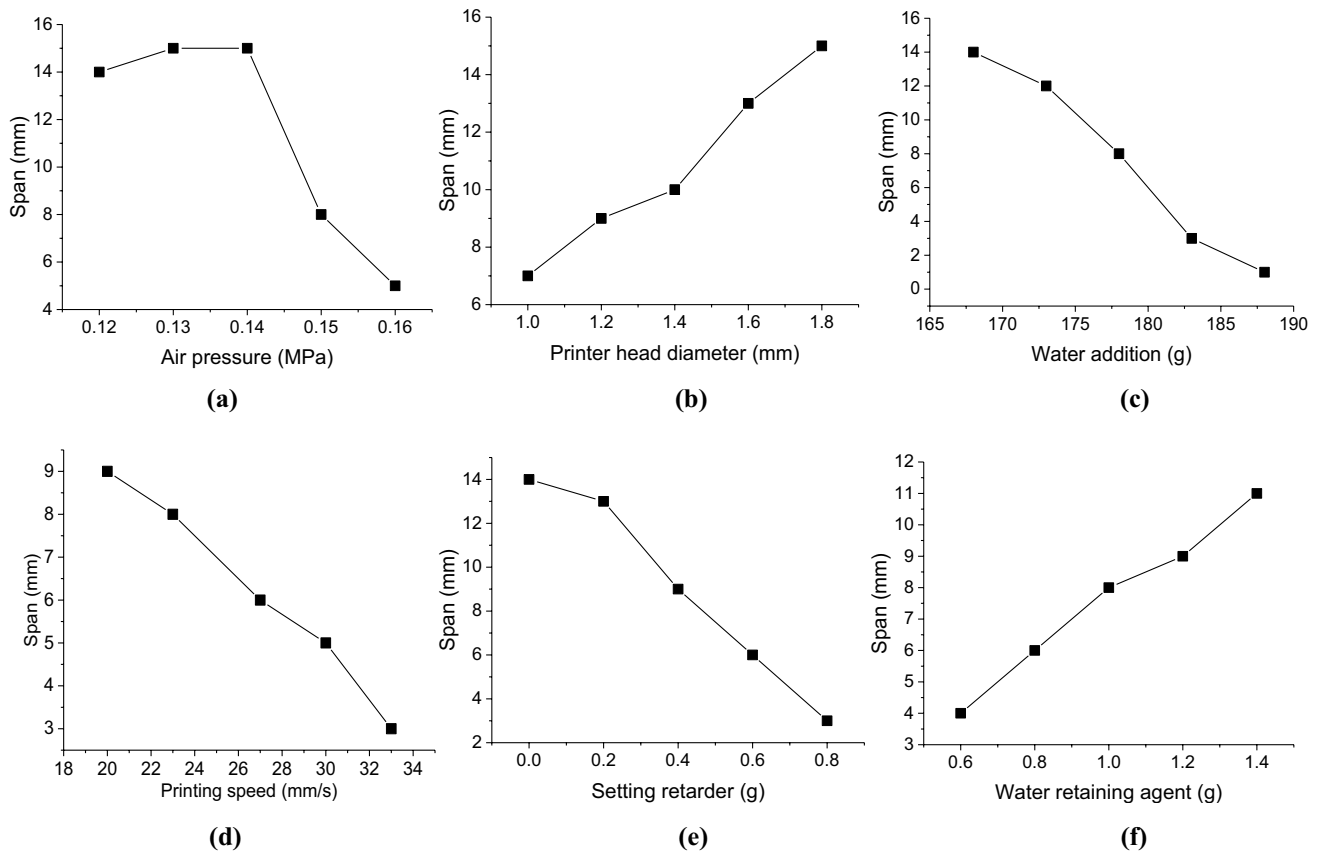


**Fig. 13** Line slump influence factor; **a** air pressure; **b** printer head diameter; **c** water addition; **d** printing speed; **e** setting retarder; **f** water retaining agent

#### 4.2.1 Surface Characteristics of Printed Samples

To investigate the surface characteristics of printed samples, four kinds of samples were printed. For printing caulking gypsum samples, the gypsum and water mass were 500 g and 150 g, respectively. For printing high-strength gypsum samples, the gypsum, water, setting retarder, and water-retaining agent weighed 500 g, 210 g, 3 g, and 1 g, respectively. For printing 325R ordinary slag Portland cement samples, the cement, water, setting retarder, and water-retaining agent weighed 500 g, 180 g, 0.8 g, and 1 g, respectively. For printing 525R ordinary Portland cement, the cement, water, setting retarder, and water-retaining agent weighed 500 g, 200 g, 0.8 g, and 1 g, respectively. The printing speeds and printer head diameters were all 60 mm/s and 1.4 mm, respectively. The size of printed specimen was 105.00 mm × 55.00 mm × 55.00 mm, and the printing direction was perpendicular to loading direction.

Figure 15 shows the surface characteristics of 3D-printed samples. Samples of A, B, C, and D were the caulking gypsum sample, high-strength sample, 325R ordinary slag Portland cement, and 525R ordinary Portland cement, respectively. Figure 15a shows that the surrounding surface

of printed samples layered; however, the top and bottom surfaces were smooth. When the printed sample surface was wire-cut, we found that the layering was not significant in the interior of printed samples (Fig. 15b). In the end, the dimension of printing specimens was measured. The size of caulking gypsum, high-strength gypsum, 325R slag Portland cement, and 525R Portland cement was 104.23 mm × 53.14 mm × 53.53 mm, 102.51 mm × 52.37 mm × 52.52 mm, 102.31 mm × 51.45 mm × 51.23 mm, and 103.34 mm × 51.51 mm × 51.72 mm. These indicated that all of printed samples occurred shrinkage.

#### 4.2.2 Application

The uniaxial compression test was performed with rockman207 hard rock triaxial testing system. During testing, the loading mode was initiated through displacement control with a ratio of 0.005 mm/s, and the axial strain was measured using a linear variable differential transformer (LVDT). The loading direction was paralleling to layer direction. The size of printed samples was rendered smooth with size of 100 mm × 50 mm × 50 mm. Figure 16a shows the uniaxial stress–strain curve of printed samples with 525R ordinary



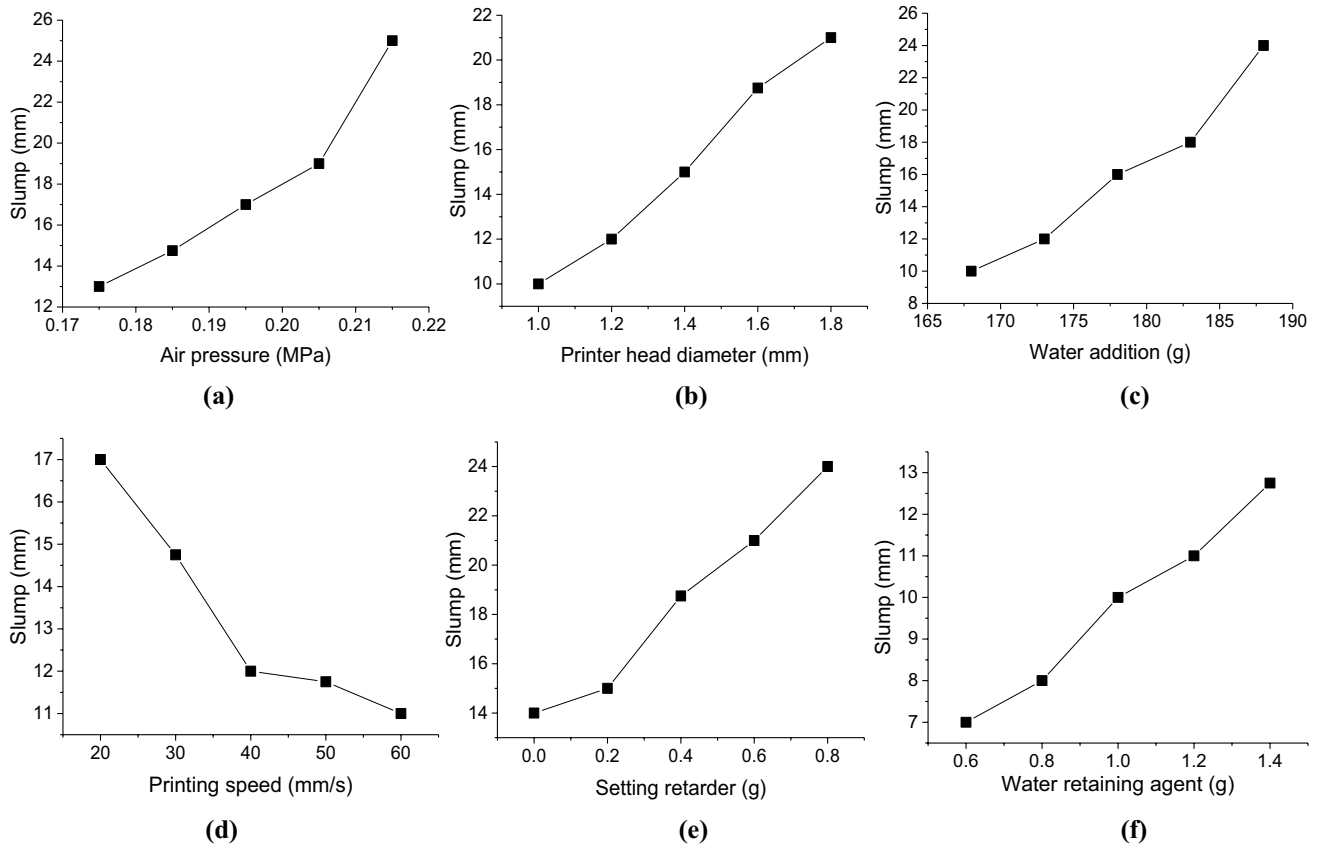


**Fig. 14** Line slump influence factor; **a** air pressure; **b** printer head diameter; **c** water addition; **d** printing speed; **e** setting retarder; **f** water-retaining agent

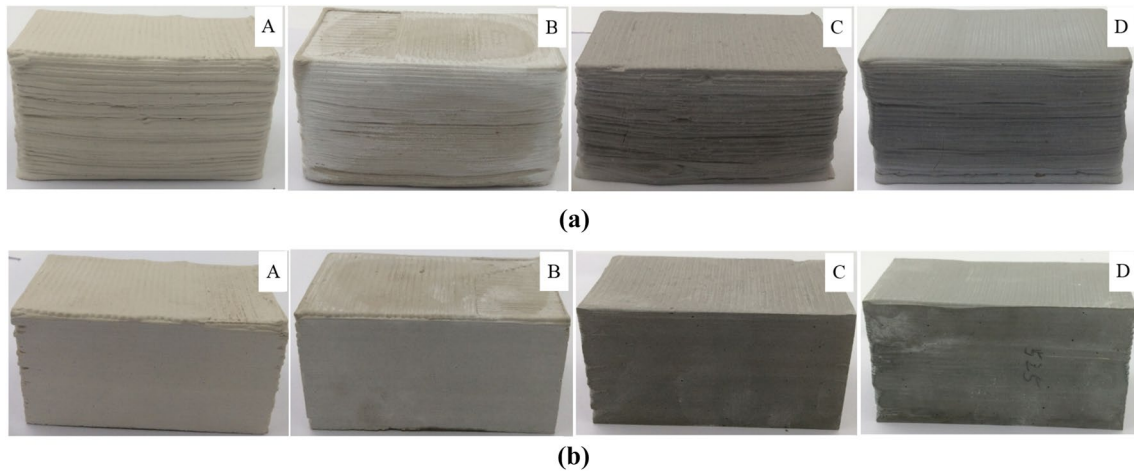


**Fig. 15** Surface characteristics of 3D-printing samples; **a** 3D-printing sample; **b** post-processing surface characteristics; A—caulking gypsum, B—high-strength gypsum, C—325R ordinary Portland cement, D—525R Portland cement

Portland cement. The axial stress increased approximately linearly with axial strain before peaking and then sharply decreased. The curve feature was similar to some layer rock, such as black shale (Chen et al. 2014), laminated sandstones

(Khanlari et al. 2015), and slate (Li et al. 2015, 2017). Figure 16b shows the failure mode of printed samples with 525R Portland cement. The failure plane was parallel to layer direction and it was similar to above-mentioned layer

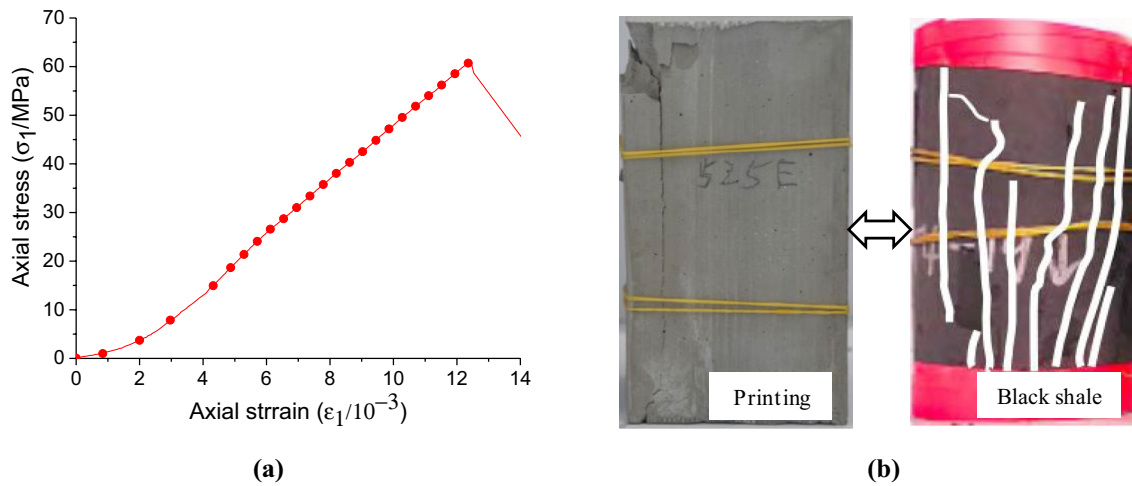


**Fig. 16** Mechanical characteristics of printed samples with 525R ordinary Portland cement; **a** uniaxial compressive strength; **b** failure mode contrast (Chen et al. 2014)

rock. In summary, the printed samples with 525R Portland cement could be used to simulate some types of bedding rock.

### 4.3 The Enlightenment for Printing Large-Scale Complex Geological Model

In upper investigation, the 3D-printing technology of geological materials, obtaining samples with desired structural and mechanical properties, was analyzed. Based on these achievements, the large-scale geological models could be printed. However, there were still some questions need to be solved: the strength of set retarder influencing, costing much printing time, complex inner structures, heterogeneity, desired density, and smooth surface. In the following section, some methods were proposed to solve these problems.

#### 4.3.1 Set Retarder Influencing and Print Time

At first, the 3D-printing technology of geological models with universal geological materials was investigated. For the 3D-printing technology, the setting retarder and water-retaining admixture were introduced to avoid rapid solidification and water segregation. To avoid blocking the pumping pipe, a longer initial setting time was required; however, when increasing setting retarder addition more than a peak value, the strength of samples would decrease (Khudhair et al. 2018; Caillaha and Moura 2018). Therefore, the setting retarder dose should be optimized properly so as to no blocking pipe and maintain a higher strength.

The costing printing time for printing samples 55 mm × 55 mm × 105 mm was almost 4 h using a 1.4 mm printer head. When the printer head diameter was 1 mm, the printing time approached 9 h. For large-scale geological

models, their dimensions often exceed 1 m. If using high-precision printing, the printing time could exceed 1 year. Therefore, some measures must be introduced to overcome this problem. One solution was that we chose a small print head for printing complex structures. When printing with no structures, we chose a bigger print head for rapid printing of geological models.

#### 4.3.2 Printing Models with Complex Structures, Heterogeneity, Desired Density, and Smooth Surface

As is known to all, most of engineering rock mass was heterogeneous and included complex structures. To get the large-scale heterogeneous geological models with complex inner structures, desired density, and smooth surface, some methods were proposed. To get large-scale heterogeneous geological models with complex inner structures, multiple print head technology that included a serial of material heads and different sizes of print head diameter were introduced. The different sizes of print head diameters were used to manufacture structures and decreasing print time. For example, the small size print head was used to print structures. When printing with no structures, the bigger print head for rapid printing of geological models was selected to accelerate printing speed. A serial of material print heads was used to fabricate heterogeneous models. For example, the fault, joints, and rock mass could be printed with its similar materials by different material print heads. The models with smooth surface and density could be realized with coaming and tighter roller. Once printed one layer, the coaming increased a certain height. Then, the tight roller moved one side to another. Because upper and down of printing models were smooth, the other face was smooth controlled by surrounding coaming. If the increased coaming height

lower than layer height, the density would increase under the tight roller pressing.

## 5 Conclusion

This paper investigates the 3D printing method and its use in fabrication of geological models using rock-like materials. Based on the flow characteristics of geological materials, a new kind of 3D printing geological material technology was formulated. Then, the technology of producing the desired structural specimens, acquiring samples with mechanical properties and cracking behaviors similar to natural rock, and printing large-scale geological models were analyzed. From these results, the main conclusions are as follows:

1. 3D-printing technology of geological materials had a principle: no losing fluidity in the printing time. Rapid solidification and water segregation were the main disadvantages of 3D printing with geological material. The use of a setting retarder and water-retaining agent could avoid the geological cementing materials suffering rapid solidification and water segregation. The mixing order of admixtures affected the initial setting time. The best mixing order for setting retarder for high-strength gypsum, 325R ordinary slag Portland cement, and 525R ordinary Portland cement was simultaneous mixing, first mixing, and later mixing. The optimal mixing order of water-retaining agent for high-strength gypsum, 325R ordinary slag Portland cement, and 525R ordinary Portland cement was first mixing, later mixing, and later mixing. The fluidity of geological materials was decreasing over time due to its continuous chemical reaction and the air pressure should be increased for compensating the decreasing fluidity.
2. The parameters of print head diameter, line width, line span, and line slump were the four key factors affecting desired structural samples. Printing resolution determined by the size of aggregates and could improve limitlessly as long as the head print diameter was five times bigger than the size of aggregate. The influencing parameters of line width were selected the values corresponded the print head diameter. The line span determined the impending length of sample inner hole. If there no hole in printing sample, the parameter did not need to be consideration. The once continuous printing height should be lower than line slump height. When approaching max line slump, the printing process should suspend until the printed parts solidified.
3. From the enlightenment of printing small-scale sample, the printing methods of complex large-scale geological models including decreasing printing time, acquiring heterogeneous geological model with inner structures,

desired density, and surrounding smooth surface were proposed. To decrease the printing time, the technology of multiple print head was adopt. When printing with no structures, the bigger printer head was selected for rapid printing. The multiple print head technology also could help to acquire homogeneous geological model and complex structures with its similar materials. The geological models with desired density and smooth surface were solved using coaming and tight roller, respectively.

**Acknowledgements** The authors acknowledge the financial support from the China Coal Research Institute under Grant no. 2017YFC0804203, the 111 Project under Grant no. B17009, the CAS Key Research Program of Frontier Sciences under Grant no. QYZDJ-SSW-DQC016, China Postdoctoral Science Foundation No. 2017M621150.

## References

- Bauyrzhan P, Jonathan C, Richard C, Gonzalo ZN (2017) 3D printed sandstone strength: curing of furfuryl alcohol resin-based sandstones. *3D Print Addit Manuf* 4:149–156. <https://doi.org/10.1089/3dp.2017.0032>
- Bryan MP, Kent MD, Rickenbach J, Rimmer G, Wilson DI, Rough SL (2015a) The effect of mixing on the extrusion–spherulisation of a micro-crystalline cellulose paste. *Int J Pharm* 479:1–10. <https://doi.org/10.1016/j.ijpharm.2014.12.028>
- Bryan MP, Rough SL, Wilson DI (2015b) Investigation of static zones and wall slip through sequential ram extrusion of contrasting micro-crystalline cellulose-based pastes. *J Non Newton Fluid* 220:57–68. <https://doi.org/10.1016/j.jnnfm.2014.08.007>
- Caillahua MC, Moura FJ (2018) Technical feasibility for use of FGD gypsum as an additive setting time retarder for Portland cement. *J Mater Res Technol* 7:190–197. <https://doi.org/10.1016/j.jmrt.2017.08.005>
- Cao RH, Cao P, Lin H, Ma GW, Zhang CY, Jiang C (2018) Failure characteristics of jointed rock-like material containing multi-joints under a compressive-shear test: experimental and numerical analyses. *Arch Civil Mech Eng* 18:784:798. <https://doi.org/10.1016/j.acme.2017.12.003>
- Chen TY, Feng XT, Zhang XW, Chao WD, Fu CJ (2014) Experimental study on mechanical and anisotropic properties of black shale. *Chin J Rock Mech Eng*. <https://doi.org/10.13722/j.cnki.jrme.2014.09.006>
- Chen Y, Zhang L, Yang B, Dong J, Chen J (2015) Geomechanical model test on dam stability and application to Jinping High arch dam. *Int J Rock Mech Min* 76:1–9. <https://doi.org/10.1016/j.ijrmm.2015.01.001>
- Chia HN, Wu BM (2015) Recent advances in 3D printing of biomaterials. *J Biol Eng* 9:1–22. <https://doi.org/10.3390/jfb9010022>
- Feng XT, Pei SF, Jiang Q, Zhou YY, Li SJ, Yao ZB (2017) Deep fracturing of the hard rock surrounding a large underground cavern subjected to high geostress: in situ observation and mechanism analysis. *Rock Mech Rock Eng* 50:2155–2175. <https://doi.org/10.1007/s00603-017-1220-4>
- Fereshtenejad S, Song J (2016) Fundamental study on applicability of powder-based 3D printer for physical modeling in rock mechanics. *Rock Mech Rock Eng* 49:2065–2074. <https://doi.org/10.1007/s00603-015-0904-x>

- Fina F, Goyanes A, Gaisford S, Basit AW (2017) Selective laser sintering (SLS) 3D printing of medicines. *Int J Pharm* 529:285–293. <https://doi.org/10.1016/j.ijpharm.2017.06.082>
- Fumagalli E (1966) Stability of arch dam rock abutments. In: *Proceedings of first ISRM congress*. Lisbon, Portugal, pp 503–508
- Gosselin C, Duballer R, Roux P, Gaudilliere N, Dirrenberger J, Morel P (2016) Large-scale 3D printing of ultra-high performance concrete—a new processing route for architects and builders. *Mater Design* 100:102–109. <https://doi.org/10.1016/j.matdes.2016.03.097>
- Huang SH, Liu P, Mokasdar A, Hou L (2013) Additive manufacturing and its societal impact: a literature review. *Int J Adv Manuf Technol* 67:1191–1203. <https://doi.org/10.1007/s00170-012-4558-5>
- Jiang C, Zhao GF (2015) A preliminary study of 3D printing on rock mechanics. *Rock Mech Rock Eng* 48:1041–1050. <https://doi.org/10.1007/s00603-014-0612-y>
- Jiang Q, Feng XT, Song LB, Gong YH, Zheng H, Cui J (2016) Modeling rock specimens through 3D printing: Tentative experiments and prospects. *Acta Mech Sin* 32:101–111. <https://doi.org/10.1007/s10409-015-0524-4>
- Jiang C, Zhao GF, Zhu J, Zhao YX, Shen L (2016a) Investigation of dynamic crack coalescence using a gypsum-like 3D printing material. *Rock Mech Rock Eng* 49:3983–3998. <https://doi.org/10.1007/s00603-016-0967-3>
- Jiang Q, Feng XT, Song LB, Gong YH, Zheng H, Cui J (2016b) Modeling rock specimens through 3D printing: tentative experiments and prospects. *Acta Mech Sin* 32:101–111. <https://doi.org/10.1007/s10409-015-0524-4>
- Jiang Q, Feng XT, Gong YH, Song LB, Ran S (2016c) Reverse modelling of natural rock joints using 3D scanning and 3D printing. *Comput Geotech* 73:210–220. <https://doi.org/10.1016/j.compgeo.2015.11.020>
- Jin T, Tian H, Gao X, Liu YL, Wang J, Chen H, Lan YQ (2017) Simulation and performance analysis of the perforated plate flowmeter for liquid hydrogen. *Int J Hydrog Energy* 42:3890–3898. <https://doi.org/10.1016/j.ijhydene.2016.09.072>
- Ju Y, Xie HP, Zheng ZM, Lu JB, Mao LT, Gao F, Peng RD (2014) Visualization of the complex structure and stress field inside rock by means of 3D printing technology. *Chin Sci Bull* 59:5354–5365. <https://doi.org/10.1007/s11434-014-0579-9>
- Ju Y, Wang L, Xie HP, Ma GW, Zheng ZM, Mao LT (2017a) Visualization and transparentization of the structure and stress field of aggregated geomaterials through 3D printing and photoelastic techniques. *Rock Mech Rock Eng* 50:1383–1407. <https://doi.org/10.1007/s00603-017-1171-9>
- Ju Y, Wang L, Xie HP, Ma GW, Mao LT, Zheng ZM, Lu JB (2017b) Visualization of the three-dimensional structure and stress field of aggregated concrete materials through 3D printing and frozen-stress techniques. *Constr Build Mater* 143:121–137. <https://doi.org/10.1016/j.conbuildmat.2017.03.102>
- Kazemian A, Yuan X, Cochran E, Khoshnevis B (2017) Cementitious materials for construction-scale 3D printing: laboratory testing of fresh printing mixture. *Constr Build Mater* 145:639–647. <https://doi.org/10.1016/j.conbuildmat.2017.04.015>
- Khanlari G, Rafiei B, Abdilor Y (2015) Evaluation of strength anisotropy and failure modes of laminated sandstones. *Arab J Geosci* 8:3089–3102. <https://doi.org/10.1007/s12517-014-1411-1>
- Khelifi H, Perrot A, Lecompte T, Rangedard D, Ausias G (2013) Prediction of extrusion load and liquid phase filtration during ram extrusion of high solid volume fraction pastes. *Powder Technol* 249:258–268. <https://doi.org/10.1016/j.powtec.2013.08.023>
- Khoshnevis B, Bekey G (2002) Automated construction using contour crafting—applications on earth and beyond. *Rapid Prototyping J* 7:32–44. <https://doi.org/10.22260/isarc2002/0076>
- Khudhair MH, El Youbi MS, Elharfi A (2018) Data on effect of a reducer of water and retarder of setting time admixtures of cement pastes and mortar in hardened stat. *Data Brief* 18:454–462. <https://doi.org/10.1016/j.dib.2018.03.050>
- Kruth JP, Leu MC, Nakagawa T (1998) Progress in additive manufacturing and rapid prototyping. *CIRP Ann Manuf Tech* 47:525–540. [https://doi.org/10.1016/S0007-8506\(07\)63240-5](https://doi.org/10.1016/S0007-8506(07)63240-5)
- Lanaro M, Forrestal DP, Scheurer S, Slinger DJ, Liao S, Powell SK, Woodruff MA (2017) 3D printing complex chocolate objects: platform design, optimization and evaluation. *J Food Eng* 215:13–22. <https://doi.org/10.1016/j.jfoodeng.2017.06.029>
- Launhardt M, Worz A, Loderer A, Laumer T, Drummer D, Hausotte T, Schmidt M (2016) Detecting surface roughness on SLS parts with various measuring techniques. *Polym Test* 53:217–226. <https://doi.org/10.1016/j.polymertesting.2016.05.022>
- Li SC, Wang Q, Wang HT, Jiang B, Wang DC, Zhang B, Li Y, Ruan GQ (2015) Model test study on surrounding rock deformation and failure mechanisms of deep roadways with thick top coal. *Tunn Undergr Sp Tech* 47:52–63. <https://doi.org/10.1016/j.tust.2014.12.013>
- Li ZG, Xu GL, Huang P, Zhao X, Fu YP (2017) Experimental study on anisotropic properties of Silurian silty slates. *Geotech Geol Eng* 35:1755–1766. <https://doi.org/10.1007/s10706-017-0206-z>
- Lille M, Nurmela A, Nordlund E, Metsä-Kortelainen S, Sozer N (2018) Applicability of protein and fiber-rich food materials in extrusion-based 3D printing. *J Food Eng* 220:20–27. <https://doi.org/10.1016/j.jfoodeng.2017.04.034>
- Liu YR, Guan FH, Yang Q, Yang RQ, Zhou WY (2013) Geomechanical model test for stability analysis of high arch dam based on small blocks masonry technique. *Int J Rock Mech Min* 61:231–243. <https://doi.org/10.1016/j.ijrmms.2013.03.003>
- Liu P, Ju Y, Ranjith PG, Zheng ZM, Wang L, Wanniarachchi A (2016) Visual representation and characterization of three-dimensional hydrofracturing cracks within heterogeneous rock through 3D printing and transparent models. *Int J Coal Sci Technol* 3:284–294. <https://doi.org/10.1007/s40789-016-0145-y>
- Ma GW, Wang L, Ju Y (2017) State-of-the-art of 3D printing technology of cementitious material—an emerging technique for construction. *Sci China Technol Sci* 61:475–495. <https://doi.org/10.1007/s11431-016-9077-7>
- Melchels FPW, Feijen J, Grijpma DW (2010) A review on stereolithography and its applications in biomedical engineering. *Biomaterials* 31:6121–6130. <https://doi.org/10.1016/j.biomaterials.2010.04.050>
- Mondschein RJ, Kanitkar A, Williams CB, Verbridge SS, Long TE (2017) Polymer structure-property requirements for stereolithographic 3D printing of soft tissue engineering scaffolds. *Biomaterials* 140:170–188. <https://doi.org/10.1016/j.biomaterials.2017.06.005>
- Otten W, Pajor R, Schmidt S, Baveye PC, Hague R, Falconer RE (2012) Combining X-ray CT and 3D printing technology to produce microcosms with replicable, complex pore geometries. *Soil Biol Biochem* 51:53–55. <https://doi.org/10.1016/j.soilbio.2012.04.008>
- Pham DT, Gault RS (1998) A comparison of rapid prototyping technologies. *Int J Mach Tool Manuf* 38:1257–1287. [https://doi.org/10.1007/978-3-319-53523-4\\_5](https://doi.org/10.1007/978-3-319-53523-4_5)
- Shakor P, Sanjayan J, Nazari A, Nejadi S (2017) Modified 3D printed powder to cement-based material and mechanical properties of cement scaffold used in 3D printing. *Constr Build Mater* 138:398–409. <https://doi.org/10.1016/j.conbuildmat.2017.02.037>
- Skawinski WJ, Busanic TJ, Ofsievich AD, Venanzi TJ, Luzhkov VB, Venazi CA (1995) The application of stereolithography to the fabrication of accurate molecular models. *J Mol Graph* 13(2):126–135. [https://doi.org/10.1016/0263-7855\(95\)00001-m](https://doi.org/10.1016/0263-7855(95)00001-m)
- Tan HB, Zhang X, Guo YL, Ma BG, Jian SW, He XY, Zhi ZZ, Liu XH (2018) Improvement in fluidity loss of magnesia phosphate cement by incorporating polycarboxylate superplasticizer. *Constr Build Mater* 165:887–897. <https://doi.org/10.1016/j.conbuildmat.2017.12.214>



- Tian W, Han NV (2017) Mechanical properties of rock specimens containing pre-existing flaws with 3D printed materials. *Strain* 53:e12240. <https://doi.org/10.1111/str.12240>
- Vogler D, Walsh S, Dombrowski E, Perras MA (2017) A comparison of tensile failure in 3D-printed and natural sandstone. *Eng Geol* 226:221–235. <https://doi.org/10.1016/j.enggeo.2017.06.011>
- Wang PT, Liu Y, Zhang L, Huang ZJ, Cai MF (2017) Preliminary study on uniaxial compressive properties of 3D printer fractured rock models: an experimental. *Chin J Rock Mechan Eng* 37:364–373. <https://doi.org/10.13722/j.cnki.jrme.2017.1039>
- Weng ZX, Zhou Y, Lin WX, Senthil T, Wu L (2016) Structure-property relationship of nano enhanced stereolithography resin for desktop SLA 3D printer. *Compos Part A Appl Sci Manuf* 88:234–242. <https://doi.org/10.1016/j.compositesa.2016.05.035>
- Xiong ZQ, Jiang Q, Gong YH, Song LB, Cui J (2015) Modeling natural joint of rock mass using three dimensional scanning and printing technologies and its experimental verification. *Rock Soil Mech* 2015:1557–1565. <https://doi.org/10.16285/j.rsm.2015.06.005> (in chinese)
- Yan X, Gu P (1996) A review of rapid prototyping technologies and systems. *Comput Aided Design* 28:307–318. [https://doi.org/10.1016/0010-4485\(95\)00035-6](https://doi.org/10.1016/0010-4485(95)00035-6)
- Yang FL, Zhang M, Bhandari B, Liu Y (2018) Investigation on lemon juice gel as food material for 3D printing and optimization of printing parameters. *LWT Food Sci Technol* 87:67–76. <https://doi.org/10.1016/j.lwt.2017.08.054>
- Zhang L, Liu YR, Yang Q (2015) Evaluation of reinforcement and analysis of stability of a high-arch dam based on geomechanical model testing. *Rock Mech Rock Eng* 48:803–818. <https://doi.org/10.1007/s00603-014-0578-9>
- Zhou T, Zhu J (2017) An Experimental Investigation of Tensile Fracturing Behavior of Natural and Artificial Rocks in Static and Dynamic Brazilian Disc Tests. *Proc Eng* 191:992–998. <https://doi.org/10.1016/j.proeng.2017.05.271>
- Zhou T, Zhu JB (2018) Identification of a suitable 3D printing material for mimicking brittle and hard rocks and its brittleness enhancements. *Rock Mech Rock Eng* 51:765–777. <https://doi.org/10.1016/j.proeng.2017.05.271>
- Zhu WS, Zhang QB, Zhu HH, Li Y, Yin JH, Li SC, Sun LF, Zhang L (2010) Large-scale geomechanical model testing of an underground cavern group in a true three-dimensional (3-D) stress state. *Can Geotech J* 47:935–946. <https://doi.org/10.1139/t10-006>
- Zhu WS, Li Y, Li SC, Wang SG, Zhang QB (2011) Quasi-three-dimensional physical model tests on a cavern complex under high in-situ stresses. *Int J Rock Mech Min* 48:199–209. <https://doi.org/10.1016/j.ijrmms.2010.11.008>

**Publisher's Note** Springer Nature remains neutral with regard to jurisdictional claims in published maps and institutional affiliations.